RESEARCH PAPER

Fundamental dynamics of flow through carbon nanotube membranes

James Cannon · Ortwin Hess

Abstract The flow of a model non-polar liquid through small carbon nanotubes is studied using non-equilibrium molecular dynamics simulation. We explain how a membrane of small-diameter nanotubes can transport this liquid faster than a membrane consisting of larger-diameter nanotubes. This effect is shown to be back-pressure dependent, and the reasons for this are explored. The flow through the very smallest nanotubes is shown to depend strongly on the depth of the potential inside, suggesting atomic separation can be based on carbon interaction strength as well as physical size. Finally, we demonstrate how increasing the back-pressure can counter-intuitively result in lower exit velocities from a nanotube. Such studies are crucial for optimisation of nanotube membranes.

Keywords Non-equilibrium molecular dynamics ·
Carbon nanotube · Membrane flow

1 Introduction

Recent advances in the production of aligned carbon nanotubes (Hinds et al. 2004; Miller et al. 2001; Sun and Crooks 2000) are opening up possibilities for the realisation of membranes. Such membranes can experience much faster through-flow than standard zeolites (Ackerman et al. 2003; Chen and Sholl 2006; Skoulidas et al. 2002), and so there is much promise for their application in filtration and molecular sorting. In order to optimise the design of such arrays and tailor to specific applications, an understanding of the transport of liquids and gases through carbon nanotubes is crucial. The behaviour of fluids flowing through nanotubes is understood to be very different to the bulk, and the use of non-equilibrium molecular dynamics (MD) simulation to study nanopore flow is well established (e.g., Duren et al. 2002a, b; Dzubiella et al. 2004; Lee and Sinnott 2004; Nagayama and Cheng 2004; Mao and Sinnott 2000; Travis and Gubbins 2000; Supple and Quirke 2003; Zhu et al. 2002).

The flow through the smallest nanotubes (<2 nm) is particularly interesting. Holt et al. (2006) demonstrated experimentally that gases can achieve incredible flow rates through a nanotube membrane composed of these diameters. Polar molecules such as water can form single chains which give rise to unusual dynamics and high flow rates (Hummer et al. 2001; Fang et al. 2008). At these diameters the structure and positioning inside the nanotube of polar and non-polar atoms alike can be highly sensitive to atomic size and temperature (Arora and Sandler 2005; Jakobtorweihen et al. 2006; Zhang et al. 2008) and this can drastically effect the diffusion of atoms inside the nanotube. Thus the transition between high and low flow rates through nanotubes is highly sensitive to the environmental conditions, and the successful realisation of nano-fludic applications will require the careful tuning of nanotubes to fit the exact conditions of operation for the results desired. This is not only the case for passive transport of molecules, but also where active pumping is utilised, whether through thermal (Shiomi and Maruyama 2009) or electrical (Joseph and Aluru 2008) means.

In order to gain an understanding of the conditions necessary for optimum flow through small-diameter nanotube membranes, we use a new non-equilibrium molecular

J. Cannon (✉) · O. Hess
Department of Physics, Faculty of Engineering and Physical
Sciences, Advanced Technology Institute, University of Surrey,
Guildford GU2 7XH, UK
e-mail: j.cannon@surrey.ac.uk

dynamics (NEMD) simulation developed at the University of Surrey to examine the fundamental flow dynamics of liquid through carbon nanotubes. Argon is chosen as the model liquid, since its reproduction through MD simulation is well established and it provides a good general and extendable model of the flow. In this study we consider the flow through a variety of small-diameter nanotubes at various temperatures and back-pressures, and demonstrate and explain the fundamental conditions necessary for enhanced flow.

This article is organised as follows: after describing the simulation setup, results are presented regarding the flow of argon through nanotubes of varying diameter, and the reasons for some of the more unusual results are explored. We then go into detail about the structure of the flow, since this plays a key role in the dynamics and fluxes observed, before finally showing how the system is sensitive to the back-pressure, and how this influences the flow. We conclude with a summary of the key points, results and implications.

2 Simulation design

All simulations conducted here make use of the NEMD software developed at the University of Surrey, capable of producing a concentration-gradient induced flow. Figure 1 shows a schematic of the design. Atoms are maintained at a constant density and temperature with zero overall momentum inside the pool, using a velocity-scaling technique. The relatively low update frequency of the pool within duel-control volume grand-canonical MD (DCV-GCMD) simulations is known to adversely influence the flow dynamics (Arya et al. 2001), so in our purely MD approach, the pool is updated and maintained at every time step. A strong concentration gradient is necessary in order to induce flow on time-scales accessible by MD, however, it is known that such studies can yield results which are comparable to experiment (Duren et al. 2002a, b).

The wall on the left of the pool is reflective in order to encourage flow in the direction of the nanotube. Upon initialisation of the simulation, only the pool exists. In this initial stage, periodic boundary conditions exist in every

Fig. 1 Schematic of the simulation system

direction in order for the desired density to be built and the system to start from equilibrium with no net momentum. Once this has been achieved, the simulation cell expands to include the nanotube and other regions for the non-equilibrium stage of the simulation.

Upon commencement of the non-equilibrium stage, the nanotube is placed at a distance from the pool in the z-direction, centred on the x and y axes. For computational reasons it is treated as a rigid structure, although this should not significantly effect the diffusion through the nanotube since the density of the atoms inside the nanotube will generally be quite high and argon–argon interactions will dominate the flow (Jakobtorweihen et al. 2005). Since the flow through the nanotube is of primary interest, a reflective wall is placed around the entrance and exit to create a membrane-like situation and ensure that atoms are limited to passing through the nanotube. Nanotube diameters ranging from 6.96 to 15.64 Å are considered.

Between the pool and the nanotube there is a flow-mix region. The length of this region is large enough to ensure that the pool has no effect on the motion of atoms through the nanotube, and a natural diffusion towards the nanotube can be reproduced. At the far end of the simulation cell is a drain, where atoms are removed from the system. Again, the exit-flow region is made long enough so that the drain does not influence the flow through the nanotube.

Unlike the longitudinal z-axis with its reflective wall on the left and drain on the right, the x and y axes have periodic boundary conditions. The x and y dimensions are 26.5 Å each, while the z dimension is 99 Å, split into lengths of 36, 18, 27 and 18 Å for the pool, flow-mix, nanotube and exit-flow regions, respectively. The z-axis is further divided into 11 bins of 9 Å length, in order to allow monitoring of variables on a spatial basis. Initial filling and equilibration of the pool lasted for 50 ps, and then the non-equilibrium phase of the simulation lasted for 20–30 ns

$$V(r) = 4\epsilon \left[\left(\frac{\sigma}{r}\right)^{12} - \left(\frac{\sigma}{r}\right)^6 \right]. \qquad (1)$$

The atoms are modelled through a Lennard Jones potential (1) with a cut-off at 12 Å, and the standard Lorentz–Berthalot (Allen and Tildesley 1987) combining rules are used to determine inter-species interaction parameters. The non-bonding parameters for carbon are known to vary with nanotube curvature due to changes in the electronic orbitals (Kostov et al. 2002). Despite this, the variation is sufficiently small over the range of diameters considered here that constant average values appropriate for the range of nanotubes included in this study can be used. The interaction parameters for argon meanwhile are well known (Verlet 1967). The parameters used in these simulations are summarised in Table 1.
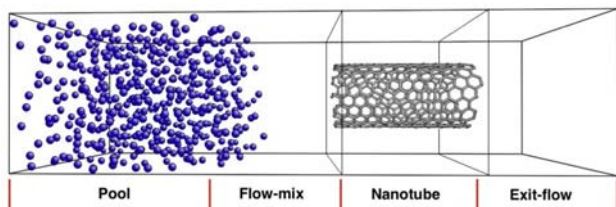
Table 1 LJ parameters used in these simulations

	ϵ (meV)	σ (Å)
Argon–argon	10.32	3.41
Carbon–carbon[a]	2.4	3.43
Carbon–argon	5.0	3.42

[a] Although the bonds between the carbon atoms were fixed, a carbon–carbon value for ϵ and σ was used to subsequently derive the inter-species interaction parameters

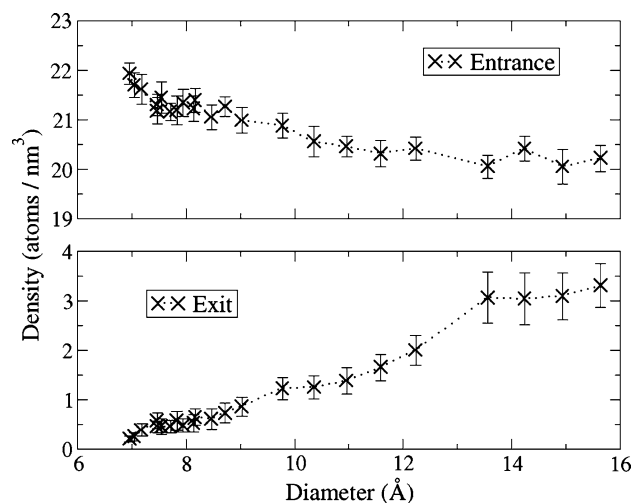## 3 Variation of flow-rate with diameter

The diameter of the nanotubes considered in this study are only marginally larger than the size of argon atoms, and therefore the dynamics of flow will depend strongly on the transient atomic structures formed. The structures and effects induced will be sensitive to the diameter of the nanotube, and so initial studies focus on this aspect.

The argon simulations were conducted with the pool at 100 K at saturated liquid density, in a subcritical state. Figure 2 shows how, as expected, there is an increase in the flow rate with diameter. In addition, however, since the atoms are free to diffuse through the nanotube, the density-drop across the nanotube is allowed to develop naturally, and thus different density-drops for the different diameters may be induced. The effect of this on the flow rate must be quantified in order to allow an analysis of the flow rate between the nanotubes of different diameters. The results show that the magnitude of the density-drop decreases with increasing diameter, and this can be explained largely by the different build-up of atoms caused by the different diameters.

Figure 3 shows how the smallest diameters experience a strong build-up of density in front of the nanotubes, since the chance that an atom will enter the nanotube is small. As the diameter increases, the build-up in front of the nanotube decreases as atoms find it easier to penetrate into


Fig. 3 The change in density at the entrance and exit across nanotubes of different diameters
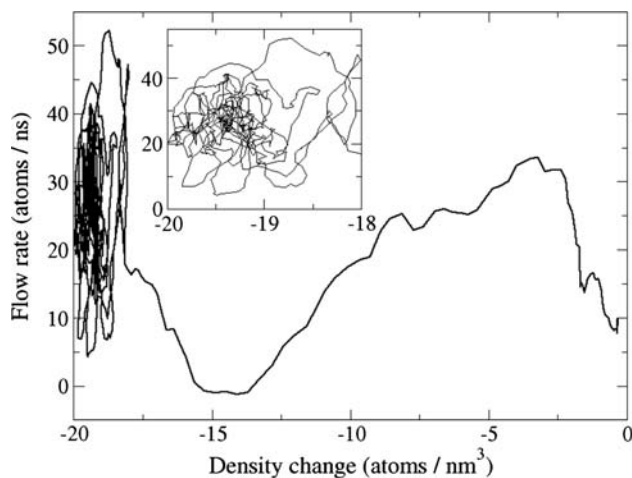
Fig. 4 The variation of flow rate and density-change across the 10.36 Å (10,5) nanotube. The simulation starts on the *right* of the graph

the nanotube. Meanwhile the opposite is the case at the exit. Here at the smallest diameters, atoms are squeezed out of the nanotube and rapidly proceed to the drain. This is in contrast to the larger nanotubes, where the atoms tend to bulge out from the exit of the nanotube slightly, in turn creating a slightly higher density. While larger density-drops are usually associated with higher flow rates, it is the opposite case here, and thus there appears to be no dependence of the flow rate on the density-drop across the nanotube. Figure 4 shows the evolution of the density-drop across the nanotube, compared to the flow rate, for the 10.36 Å (10,5) nanotube, demonstrating the independence of the two quantities.

Given that the density-drop does not appear to play a significant role in the rate of flow through the nanotube,


Fig. 2 Variation of argon flow rate with diameter
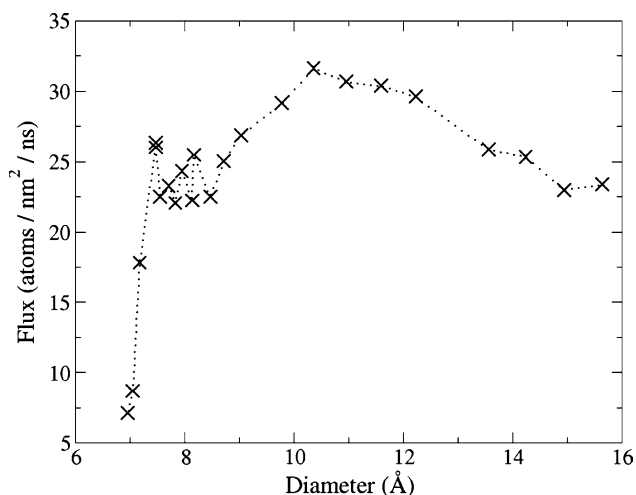
Fig. 5 The variation of argon flux with diameter

Fig. 6 An equilateral triangle taken from an ideal hexagonal packing of nanotubes

calculation of the transport-diffusion coefficient through Fick's law, for example, would be inappropriate. What, however, is important is the rate of flow relative to the cross-sectional area of the nanotube. Thus the flux through the nanotube (rate of flow per unit cross-sectional area, based upon the carbon atom-centre diameter) can be calculated, and this is shown for the full range of diameters in Fig. 5.

This highlights a number of points. Firstly the squeezing and prevention of flow in the smallest nanotubes is clearly visible, and as the diameter increases the flux rapidly increases too. Following this the flux remains constant at around 22–26 atoms nm^{-2} ns^{-1} as the diameter increases. The flux then rises steadily again, reaching a peak at around 10–11 Å, before steadily decreasing back to the 22–26 atoms nm^{-2} ns^{-1} range.

It is clear that while the rate of flow is higher for larger nanotubes, the flux is higher for nanotubes around 1nm in diameter. In terms of experiment and application, what is important is not so much the flux through an individual nanotube, but whether an increase in the flow rate can be achieved by using a larger number of small nanotubes, or a smaller number of large nanotubes. The larger nanotubes have a lower flux, but less "dead" surface area caused by the presence of the carbon atoms. While the flow and flux through a single nanotube has often been studied, this rate of flux through a membrane has not, to our knowledge, been considered in this way before. This is, however, the key quantity needed in the design and application of membranes.

Thus the calculation can be extended to a membrane in the following way. Assuming the nanotubes maintain a perfectly circular cross-section, the optimal packing of the nanotubes is a hexagonal array. The fabrication of a nanotube membrane would involve millions of tightly
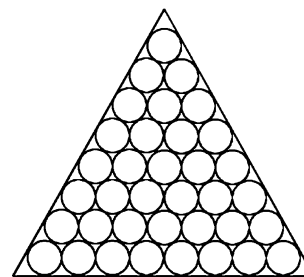
packed nanotubes. In the present calculation, an equilateral triangle is taken out of this hexagonal array (Fig. 6), consisting of 1,000 nanotubes on each side of the triangle, giving a total of 500,500 nanotubes. The minimum distance between each of these nanotubes is given by the value of σ_{C-C} of 3.43 Å introduced earlier. Thus half of this is added to the effective radius of each nanotube. Overall, the dead surface area is relatively larger for the smaller nanotubes, compared to the larger ones. Knowledge of the number of nanotubes along the side of the triangle (N_s), each with radius r, allows the length of the side of this triangle (L_s) to be calculated through Eq. 2, which in turn allows the surface area of the triangle to be calculated. The edge of the triangle is slightly difficult to define and leads to a slight overestimation of its area, however, for the current approximation, by taking such a large number of nanotubes, the overall effect of this can be minimised. The flux through the triangle can then be found, given the surface area of the triangle, the number of nanotubes, and the expected rate of flow through all the nanotubes. Figure 7 shows this for each nanotube diameter.

$$L_s = (2(N_s - 1) + 2\sqrt{3})r. \tag{2}$$

It is clear that despite the relative increase in the dead surface area, the medium-size nanotubes studied here would produce a membrane which is capable of transmitting atoms around 15% faster than the larger nanotubes. This is a significant result, since such enhancements in flow would be very useful when considering filtration or other applications. In order to decipher why some smaller nanotubes have a higher flux than larger nanotubes, the structure and dynamics of the flow must be understood. This is discussed in the following section.

4 Flow structure

The range of diameters showed a significant variation in the flux, and much of this can be attributed to the structure
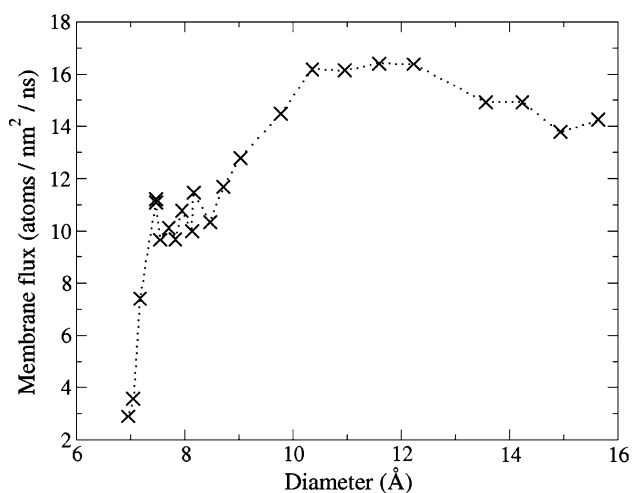
**Fig. 7** The variation of argon flux with nanotube diameter, through a 500,500-nanotube triangular membrane

Fig. 8 Increasing the interaction strength of the carbon atoms causes the central potential well within the nanotube to deepen. The subsequent increase in flow rate is seen to match well with the increase that would have been observed if the increase in the depth of the potential had been caused by an increase in diameter instead

of flow inside the nanotube. This section discusses the structure and its implications in full detail.

4.1 The smallest diameters

The smallest diameters studied are those through which argon can barely pass. The value of σ_{C-Ar} is 3.42 Å, and thus for entrance into the nanotube, the diameter must have at least twice this value. This compares with the minimum diameter nanotube used in this study of 6.96 Å; barely big enough for argon to fit. This is why the flux drops very quickly at these tiny diameters.

A potential well is formed in the centre of these small nanotubes, and as the diameter increases the depth and width of this well also increases. The smallest 5 nanotubes have a fairly linear increase in the flow rate and flux with diameter, with correlation coefficients of 0.987 and 0.986, respectively. In addition, the flow rate also corresponds very closely to the depth of the central potential well in these nanotubes with a correlation coefficient of 0.999, and it is interesting to consider what role this increasing potential well plays in the substantial increase in the flow rate that is observed.

In order to test this, the 7.05 Å-diameter (9,0) nanotube was considered and the interaction strength of the carbon atoms increased by 25 and 50% in two different simulations. This causes the potential in the centre of the nanotube to become deeper, while the well-width remains the same. Figure 8 demonstrates how this results in an increase in the flow rate too. In fact, the figure shows that the increase in flow rate matches well with the increase that would have been observed had the increase in the depth of the potential been caused by an increase in diameter instead. Therefore it can be suggested that the
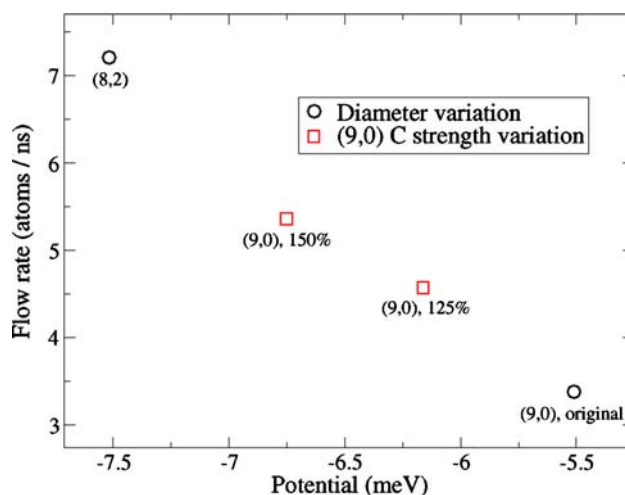
increase in diameter is playing only an indirect role in the changes in the flow rate, and in fact it is the depth of the potential inside the nanotube which is playing a defining role.

The significant change in flux experienced by just a small change in the diameter could be of substantial interest for separation experiments. If two species are to be separated which have slightly different interaction ranges, then the precise diameters at which the potential reaches a maximum will be different for each species and a strong selectivity of the species could be obtained. These results also show that this could furthermore be used to separate species which have a similar "size", but different interaction energies. The difference in the interaction energies would only have to be small to generate a significant difference in the flow rate.

4.2 Constant flux

It has been described in the previous section how the very smallest diameters, from 6.96 to 7.47 Å, are subject to a potential with a minimum in the centre of the nanotube which increases as the diameter increases. Eventually though, due to the shape of the LJ potential, the potential stops becoming deeper, reaching a maximum depth of almost −10 meV with the 7.71 Å nanotube. As the diameter continues to increase to 8.72 Å the potential slowly becomes flatter and wider, and rises slightly to almost −7 meV. The point of deepest potential remains in the centre of the nanotube, until it flattens out and a minor central bump in the potential (less than 0.1 meV in magnitude) can be observed. Figure 5 shows that this region

from 7.47 to 8.72 Å corresponds to a region of constant flux.

Over this range of nanotubes the number of atoms that can fit inside the nanotube at any one time is constant. This, in combination with the relatively flat central potential, means that the only changing parameter is the diameter of the nanotube. Thus the increase in the flow rate (and hence constant flux) is due to the fact that the chance for entry by atoms into the nanotube increases with diameter. This is very different to the smallest nanotubes where the depth of the potential played a significant role. The constant flux region ends when the structure within the nanotube changes from single-file to strongly zig-zag and the number of atoms inside the nanotube increases.

4.3 The medium diameters

The medium diameters see a marked increase in the number of atoms that are able to fit into the nanotube, and this is accompanied by an increase in the flux. The flux increase continues to 31.5 atoms nm^{-2} ns^{-1} at the 10.36 Å nanotube, giving unusually high flux, before decreasing again.

Figure 9 shows how the density inside the different nanotubes varies with diameter. The smallest nanotubes can only fit one strand of atoms inside, and since the number of atoms inside these nanotubes remains constant, as the diameter increases, the density inside reduces. At 9.78 Å, two clear strands are able to fit inside and so a sudden increase in the density is observed. The diameter of highest flux at 10.36 Å continues this increase in density with three strands inside. Therefore the rapid increase in density for the relatively small diameter plays an important role in giving the 10.36 Å nanotube (and its neighbours) an unusually high flux.
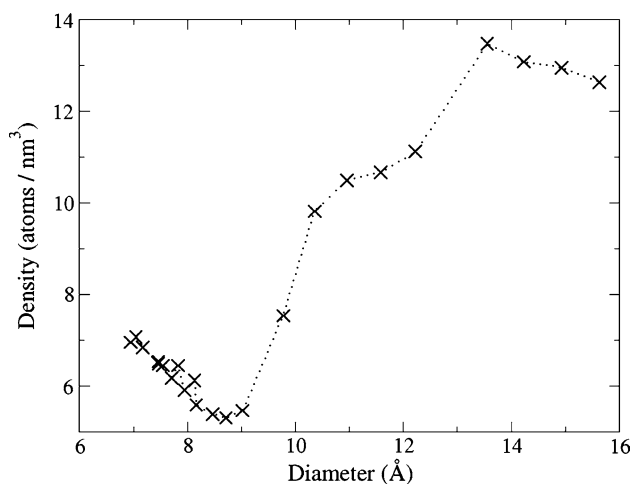
Fig. 9 The variation of density inside the nanotubes with diameter
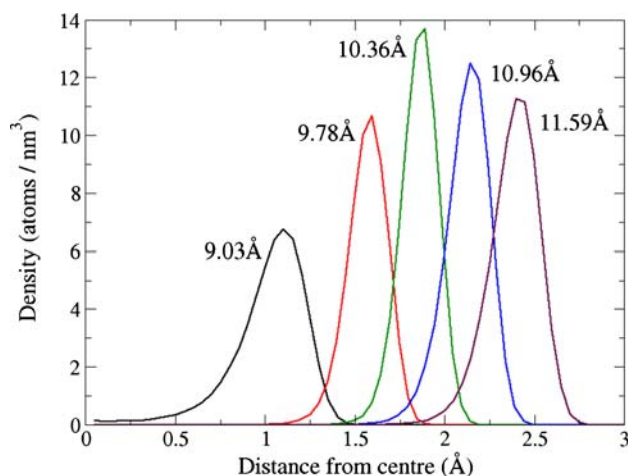
Fig. 10 The radial density distribution of the atoms in different nanotube diameters. The diameter of highest flux (10.36 Å) shows the *tallest peak*, with consecutively smaller and consecutively larger diameters shown with *peaks to the left* and *right*, respectively

This is not the whole story, however, since the well-defined structure arising from the confinement also helps to encourage fast transport. The radial density of the 10.36 Å nanotube displays a peak which is sharper and taller than for neighbouring diameters (Fig. 10), suggesting that the structure is better-defined inside the 10.36 Å nanotube compared to its neighbours. The less-well defined flow structure in the larger 10.96 and 11.59 Å nanotubes exists despite an increase in the density inside the nanotubes.

An increase in the number of helix strands is also observed: 4 strands for the 11.59 Å-diameter nanotube, and 5 for the 12.23 Å-diameter nanotube. Thus the looser flow-structure in combination with the driving force being spread out over a greater number of strands contributes to an overall decrease in the flux. The average velocity inside the 10.36 Å nanotube is about 14% higher compared to its three larger neighbours with similar density.

The well-defined flow structure of the 10.36 Å nanotube is also demonstrated clearly when compared to its smaller neighbour. Figure 11 shows the that while the 10.36 Å nanotube forms and maintains a 3-helix-strand structure, its smaller neighbour experiences flow which is far more chaotic, sometimes forming 2-strand helix structures, straight flow lines, or no structure at all. This is reflected closely by the central-nanotube argon–argon radial distribution function (RDF), which shows a well-defined structure for the 10.36 Å nanotube compared to the 9.78 Å nanotube (Fig. 12).

4.4 Largest diameters

The largest diameters see a significant change in the structure of flow and there are a number of characteristics which set them apart from the smaller diameters described
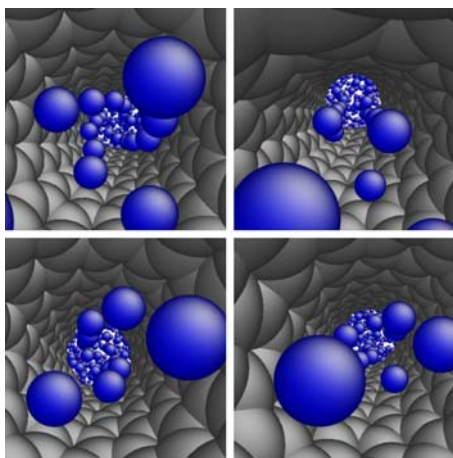
Fig. 11 *Top-left* the consistent 3-strand structure of the (10,5) 10.36 Å-diameter nanotube. The *other three panels* illustrate the various structures within the (10,4) 9.78 Å-diameter nanotube showing straight-flow (*top right*), double-helix flow (*bottom left*) and unstructured flow (*bottom right*)
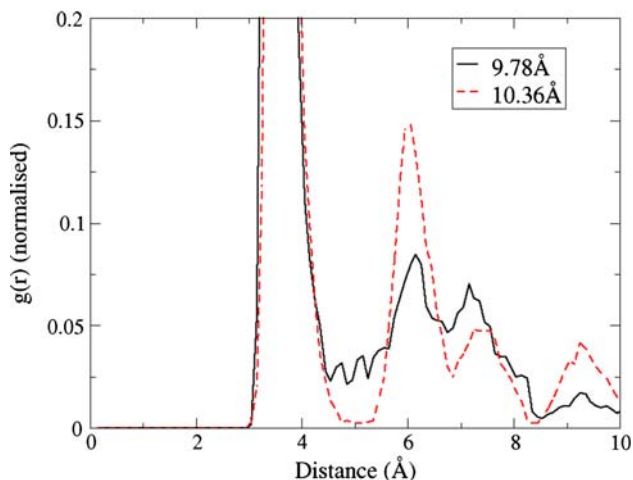
Fig. 12 The radial distribution function for the diameter of highest flux (10.36 Å) and its smaller neighbour for comparison

up until now. Firstly, the flow rate is seen to flatten-out (Fig. 2), and the flux returns to the levels seen earlier in the constant-flux diameters. The structure changes significantly too: in addition to the helix strands around the inner-wall of the nanotube, the diameter is now large enough to accommodate a single straight strand of atoms down the centre. This is most pronounced in the 13.56 Å nanotube, and becomes less pronounced and more spread-out as the diameter increases further, until the central strand eventually splits into a zig-zag formation about the centre.

For these four largest nanotubes, the increase in the number of atoms in the nanotube is linear. The increase in the overall flow rate is not strictly linear, however, and hesitates in the second-largest (14.94 Å) nanotube. This is reflected in the structure, revealed through analysis of the
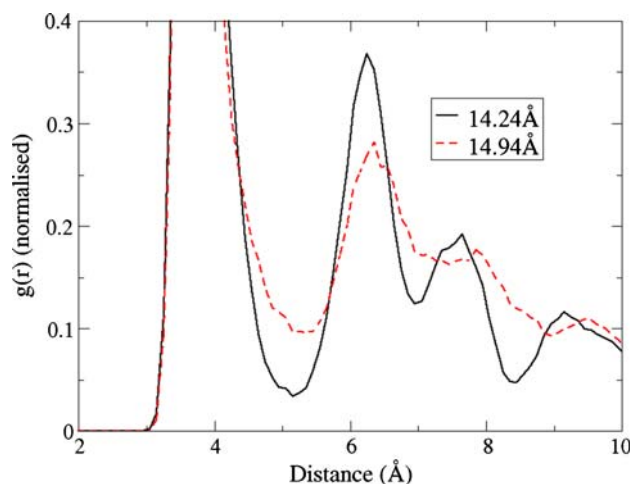
Fig. 13 The RDF inside the 14.24 and 14.94 Å nanotubes, *highlighting* the clearer structure of the smaller nanotube

in-nanotube RDF (Fig. 13), showing how this nanotube displays less structure inside than its smaller 14.24 Å neighbour. The structure within the 14.24 Å allows an average 9% increase in the flow velocity within the nanotube, over it's slightly larger 14.94 Å neighbour, therefore again adding weight to the findings that clearer structure helps enhance flow rates.

Finally it is important to note that the dynamics of flow through these larger nanotubes are very different to the smaller nanotubes studied up until now, due to the presence of the central strand which induces "falling dynamics". While an ejected atom would be unlikely to return to the nanotube if the nanotube were small, it is very common for an atom which is initially ejected from an outer helix strand of a large nanotube to fall into the central strand of the nanotube, rather than escaping, reducing the overall rate of ejection of atoms from the nanotube, and causing the slight flattening of the flow rate shown earlier in Fig. 2.

5 Variation in pool density

While the previous section gives an insight into the influence of the diameter on the flow rate, it is also important to consider what happens if the back-pressure changes in magnitude. By forcing the atoms through the nanotube at a different rate, any change in the structure and dynamics of flow can be investigated.

5.1 Experimental set-up

In the previous section, the pool contained 500 atoms at 100 K. Given the dimensions of the pool, the resultant argon density is 1,311 kg m^{-3}, which represents the liquid saturated density. The maintenance of the pool at this

density forms a back-pressure which drives the atoms forward and through the nanotube. In order to vary this back-pressure and test what effect it has on the flow, the density of the pool was tested at 400, 450, 475, 525 and 550 atoms, in addition to the density of 500 atoms already performed. The RDF of the pool at these densities was checked, confirming that it is still in the liquid phase.

It was found with 400 and 450 atoms in the pool, with a density of 1,049 and 1,180 kg m^{-3}, respectively, that the argon liquid coagulated in the pool, and very little flow occurred; the back-pressure was almost zero. In the case of the larger diameters which can accommodate more atoms than the smaller diameters, the filling time became prohibitively long for the 400 and 450-atom pools, and so these were not considered further.

Testing the different diameters at different pool densities required a large amount of computational time, and therefore the number of diameters tested was reduced, while ensuring to keep the range large and to include the diameter of highest flux from the previous study.

5.2 Key results

A key result of the previous section was the enhanced flux observed at medium diameters. It is important therefore to consider whether this result holds at higher back-pressures too, or if it is back-pressure dependent. Figure 14 shows that while the 10.36 Å nanotube retains its position as the diameter of highest flux for the 475 pool, it fails to do so for the 525 and 550 pools. This is significant, for if the maximum flow rate were desired, different diameter nanotubes would be appropriate for different back-pressures.

In order to study further into the mechanisms behind this sudden change, the density drop across the nanotube was
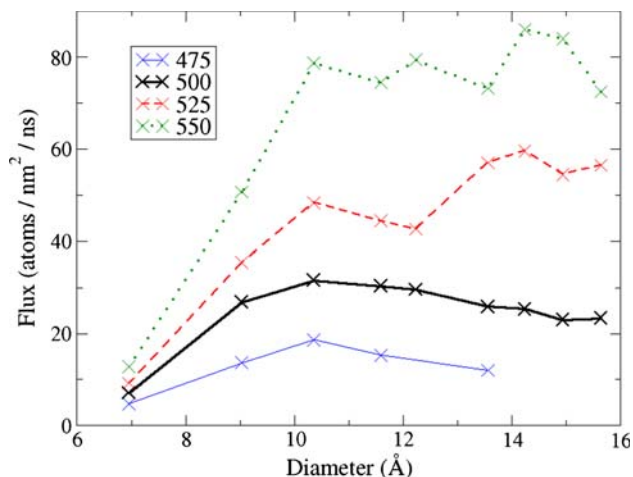
Fig. 14 The variation of flux with diameter for different pool densities
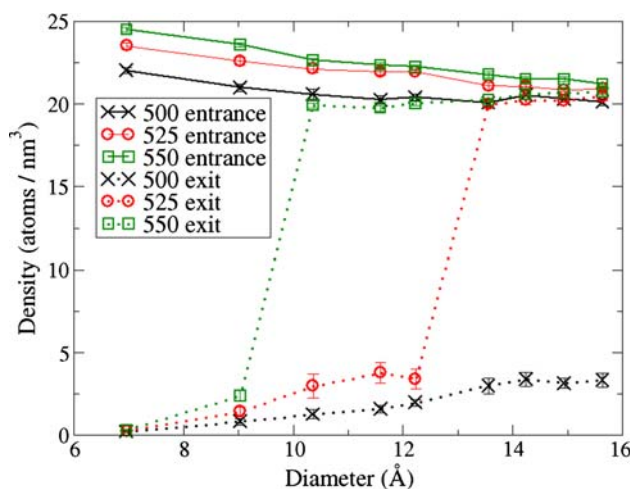
Fig. 15 The variation of density with diameter for different pool densities

also considered. With a higher flow rate towards the nanotube, it would be expected that the density in front of the nanotube increases slightly, and thus the density-drop across the nanotube would be greater. Figure 15 shows that while the density at the entrance of the nanotube increases as expected, the density at the exit increases very suddenly above 13.56 and 10.36 Å for the 525 and 550 pools, respectively, resulting in a catastrophic collapse in the density-drop across the nanotube.

This result is not immediately intuitive, and closer examination reveals that from the minimum diameters of unusual density-change, the flux also experiences an unusual increase, which removes the 10.36 Å diameter from its previous role of highest-flux.

5.3 Analysis

Overall, the density-change corroborates earlier findings of an inverse correlation between the density-change and the flow rate. It was also found earlier, however, that the density-drop actually played no role in the flow rate, and so it must be considered here whether the correspondence between the collapse of the density-drop and the increase in the flux has a cause and effect relationship, or whether, like before, they are independent of each other.

Taking the flow through the 13.56 Å-diameter nanotube for example, the 525-atom pool results in a weak density-drop. In this particular case the density outside the exit of the nanotube increases steadily from around 0.75 ns, until reaching its maximum at 7 ns. Considering the flow during this period, if the density outside the exit of the nanotube is playing a role in the enhanced flow rate, then the flow rate would be expected to increase steadily, coming to a constant value around 7 ns. This is, however, not the case, and the flow rate is established almost immediately. Thus it
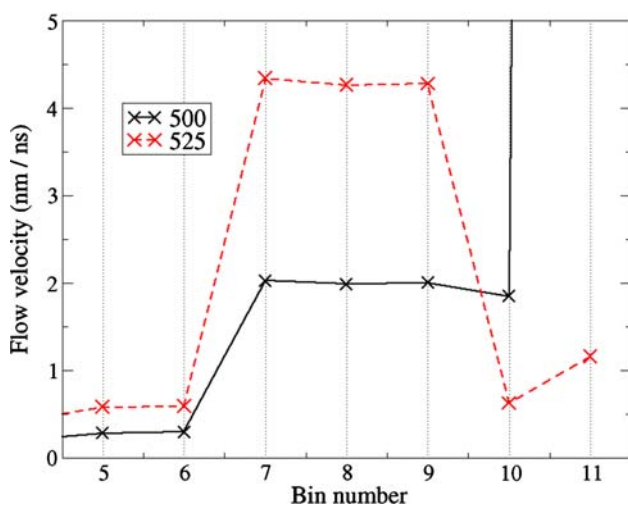
does not appear that the density outside the exit of the nanotube is playing a role in the enhanced flow rate.

Another important prospect could be a change in the structure of flow within the nanotube. In particular, a breakdown in the structure would herald an important transition inside the nanotube, whether in terms of phase or simply new flow-structures more suited to the back-pressure applied. Reviewing the RDF, radial structure and number of atoms within the nanotube reveals no structural change, however, so this is not the cause of the change of the flow rate either.

What is seen to change, however, is the velocity inside the nanotubes. All nanotubes experience this increase in velocity, whether they are subject to the unusual density-change or not. The increase in velocity is also fully radial, and even the larger nanotubes which are able to fit a strand of atoms down the centre as well as round the edge see an increase across the whole radius. Furthermore, the velocity outside the nanotube changes dramatically, and this is particularly noteworthy since it gives an important insight into the dynamics and reasons for the collapse in the density-drop. Figure 16 shows the average atomic flow velocity across the z-axis of the simulation cell for the 13.56 Å nanotube at 500 and 525 pool atoms, giving the non-enhanced and enhanced flow, respectively.

In the case of the 500-atom pool, the atoms find it difficult to escape the nanotube, and so when they do, it is at high velocity and the overall flow is generally only in one direction ($+z$). A few atoms that exit the nanotube are pulled back and remain around the nanotube exit for a slightly extended period of time, and this serves to slightly

moderate the average velocity in the bin immediately outside the nanotube (bin 10). The final bin (11), however, sees an exclusive flow in the $+z$ direction and thus the overall flow here is very sparse with fast atoms.

This changes for the case of the 525-atom pool. Here the velocity of the atoms is higher and so they can pass through the nanotube much more easily. This velocity increase is only an incremental change, and thus, while atoms are able to flow more easily, their kinetic energy is such that they are still strongly influenced by the nanotube, so although they are able to exit the nanotube, many are pulled back again. This bulging out from the nanotube is what causes the increase in the density outside the exit. This in turn causes the lower flow velocities outside in bin 10, since there are many atoms which are attracted back towards the nanotube exit, although the net velocity is of course still in the $+z$ direction.

Logic therefore follows that an even stronger back pressure could eventually cause another transition in the flow, where the velocities are so high that the atoms are able to overcome the back-attraction of the nanotube and higher velocities in bin 10 are observed again whilst still maintaining the small density drop across the nanotube.

The minimum diameter from which the unusual increase in flux and density-drop is observed is greater for the 525 pool (13.56 Å+) compared to the 550 pool (10.36 Å+). This gives a hint as to why it is the larger nanotubes which display the unusual changes in flux and density-drop first. The larger the nanotube is, the greater the dominance of argon–argon interaction over argon–carbon interaction. Therefore the kinetic energy required to overcome the interaction with the nanotube is lower at larger diameters, and thus they display this transition at lower back-pressures. Secondly, the larger cross-sectional area of the larger diameters means that there is greater interaction between argon atoms inside and outside the nanotube. This in turn means that a larger back-pressure exerts more of an influence on the atoms inside the nanotube and the resulting increase in flux is observed earlier.

6 Conclusion

The flow dynamics of a model non-polar liquid through very small nanotubes has been studied using a new non-equilibrium MD simulation. We have demonstrated how, below a certain value in the back-pressure, the flux through a membrane made of 10 Å-diameter nanotubes is 15% greater than that through a membrane of 16 Å-diameter nanotubes. It has been seen how a combination at small diameters of high density with an ability to form a stable, well-defined flow-structure, is crucial in the attainment of this enhanced flux.

Fig. 16 The average flow velocity of atoms through the 13.56 Å nanotube for pool densities of 500 and 525. *Bin 11* for the 500-atom pool reaches 69 nm ns^{-1} and is not shown for clarity. *Bins 7*, *8* and *9* represent the nanotube split into thirds, while the final two bins represent the exit-flow region and *bins 5* and *6* represent the flow-mix region

The flow through the very smallest nanotubes has also been discussed. The flux through these nanotubes is highly sensitive to diameter changes, and thus they may form an integral part of atomic separation technologies. We have shown how the depth of the potential in the centre of the nanotube plays a key role in deciding the flow rate, and thus the separation of atomic species can be either by size or interaction strength.

The largest diameters considered in this study have been shown to display a very different structure with a line of atoms down the centre. The transition to "falling dynamics" with atoms from the outer strands falling into the central strand, in combination with a concentration of the back-pressure across a larger area, has been shown to somewhat hinder the rate of flow. Again, the ability to form a clear and consistent structure in the flow has been attributed to higher flow rates.

The highly counter-intuitive variation of flux with diameter has been found to change dramatically at higher back-pressures. Above a certain transition point in the back-pressure, the largest nanotubes experience the highest flux. This has been shown to be because the kinetic energy of the atoms is above a minimum energy required to overcome the interaction with the nanotube, which is lower for larger nanotubes. While this leads to an enhanced flow rate inside the nanotube, it in turn leads to a "leaking" out from the nanotube exit, rather than the high-velocity "squeezing" seen at lower back-pressures. This means that a higher back-pressure can, somewhat counter-intuitively, cause a lower average exit velocity. Another characteristic of this transition is a collapse in the density-drop across the nanotube caused by atoms having enough kinetic energy to bulge out of the nanotube, although the density-drop across the nanotube has been shown to play no role in the flow rate through the nanotube.

Overall, these results highlight the importance of simulation in the optimisation of nanofluidic applications using nanotubes.

References

Ackerman DM, Skoulidas AI, Sholl DS, Johnson JK (2003) Diffusivities of ar and ne in carbon nanotubes. Mol Simul 29(10–11):677–684

Allen MP, Tildesley D (1987) Computer simulation of liquids. Clarendon Press, Oxford

Arora G, Sandler SI (2005) Air separation by single wall carbon nanotubes: Thermodynamics and adsorptive selectivity. J Chem Phys 123(4):044,705

Arya G, Chang HC, Maginn EJ (2001) A critical comparison of equilibrium, non-equilibrium and boundary-driven molecular dynamics techniques for studying transport in microporous materials. J Chem Phys 115(17):8112–8124

Chen HB, Sholl DS (2006) Predictions of selectivity and flux for ch4/h-2 separations using single walled carbon nanotubes as membranes. J Memb Sci 269(1–2):152–160

Duren T, Keil FJ, Seaton NA (2002a) Composition dependent transport diffusion coefficients of ch4/cf4 mixtures in carbon nanotubes by non-equilibrium molecular dynamics simulations. Chem Eng Sci 57(8):1343–1354

Duren T, Keil FJ, Seaton NA (2002b) Molecular simulation of adsorption and transport diffusion of model fluids in carbon nanotubes. Mol Phys 100(23):3741–3751

Dzubiella J, Allen RJ, Hansen JP (2004) Electric field-controlled water permeation coupled to ion transport through a nanopore. J Chem Phys 120(11):5001–5004

Fang HP, Wan RZ, Gong XJ, Lu HJ, Li SY (2008) Dynamics of single-file water chains inside nanoscale channels: physics, biological significance and applications. J Phys D Appl Phys 41(10):103,002

Hinds BJ, Chopra N, Rantell T, Andrews R, Gavalas V, Bachas LG (2004) Aligned multiwalled carbon nanotube membranes. Science 303(5654):62–65

Holt JK, Park HG, Wang YM, Stadermann M, Artyukhin AB, Grigoropoulos CP, Noy A, Bakajin O (2006) Fast mass transport through sub-2-nanometer carbon nanotubes. Science 312(5776):1034–1037

Hummer G, Rasaiah JC, Noworyta JP (2001) Water conduction through the hydrophobic channel of a carbon nanotube. Nature 414(6860):188–190

Jakobtorweihen S, Verbeek MG, Lowe CP, Keil FJ, Smit B (2005) Understanding the loading dependence of self-diffusion in carbon nanotubes. Phys Rev Lett 95(4):044,501

Jakobtorweihen S, Keil FJ, Smit B (2006) Temperature and size effects on diffusion in carbon nanotubes. J Phys Chem B 110(33):16,332–16,336

Joseph S, Aluru NR (2008) Why are carbon nanotubes fast transporters of water? Nano Lett 8(2):452–458

Kostov MK, Cheng H, Cooper AC, Pez GP (2002) Influence of carbon curvature on molecular adsorptions in carbon-based materials: a force field approach. Phys Rev Lett 89(14):146,105

Lee KH, Sinnott SB (2004) Computational studies of non-equilibrium molecular transport through carbon nanotubes. J Phys Chem B 108(28):9861–9870

Mao ZG, Sinnott SB (2000) A computational study of molecular diffusion and dynamic flow through carbon nanotubes. J Phys Chem B 104(19):4618–4624

Miller SA, Young VY, Martin CR (2001) Electroosmotic flow in template-prepared carbon nanotube membranes. J Am Chem Soc 123(49):12,335–12,342

Nagayama G, Cheng P (2004) Effects of interface wettability on microscale flow by molecular dynamics simulation. Int J Heat Mass Transf 47(3):501–513

Shiomi J, Maruyama S (2009) Water transport inside a single-walled carbon nanotube driven by a temperature gradient. Nanotechnology 20(5):055,708

Skoulidas AI, Ackerman DM, Johnson JK, Sholl DS (2002) Rapid transport of gases in carbon nanotubes. Phys Rev Lett 89(18):185,901

Sun L, Crooks RM (2000) Single carbon nanotube membranes: a well-defined model for studying mass transport through nanoporous materials. J Am Chem Soc 122(49):12,340–12,345

Supple S, Quirke N (2003) Rapid imbibition of fluids in carbon nanotubes. Phys Rev Lett 90(21):214,501

Travis KP, Gubbins KE (2000) Poiseuille flow of lennard-jones fluids in narrow slit pores. J Chem Phys 112(4):1984–1994

Verlet L (1967) Computer experiments on classical fluids. I. Thermodynamical properties of Lennard–Jones molecules. Phys Rev 159(1):98

Zhang ZQ, Zhang HW, Zheng YG, Wang L, Wang JB (2008) Gas separation by kinked single-walled carbon nanotubes: molecular dynamics simulations. Phys Rev B 78(3):035,439

Zhu FQ, Tajkhorshid E, Schulten K (2002) Pressure-induced water transport in membrane channels studied by molecular dynamics. Biophys J 83(1):154–160